# Non-Parametric Stellar Brightness Profiles from Microlensing Fold Caustics

Vasileios Kalaitzidis[1]

1. School of Physics & Astronomy, University of St Andrews

## Introduction

- **Gravitational Lensing:** Light from a distant source is bent by an intermediate massive object (lens), altering its apparent **position, shape, and brightness**
- **Microlensing:** **Images are not resolvable**, but the **magnification is measurable**
- **Applications of Microlensing:** 1. Exoplanet Detection 2. Dark Matter Constraints 3.Stellar Atmospheres 4.MACHO Detection 4.Cosmology/Distances
- **Caustics:** Curves where light magnification becomes **infinite for a point source**
- **Caustic Crossings:** Source passes caustic -- **sharp brightness increase (0<η<2)**
- **Caustic Flux:** well defined shape – single dependance→ $\xi(r)$ intensity profile
- **Limb Darkening:** Differential magnification across star's surface→ $\xi(r)$ measurements

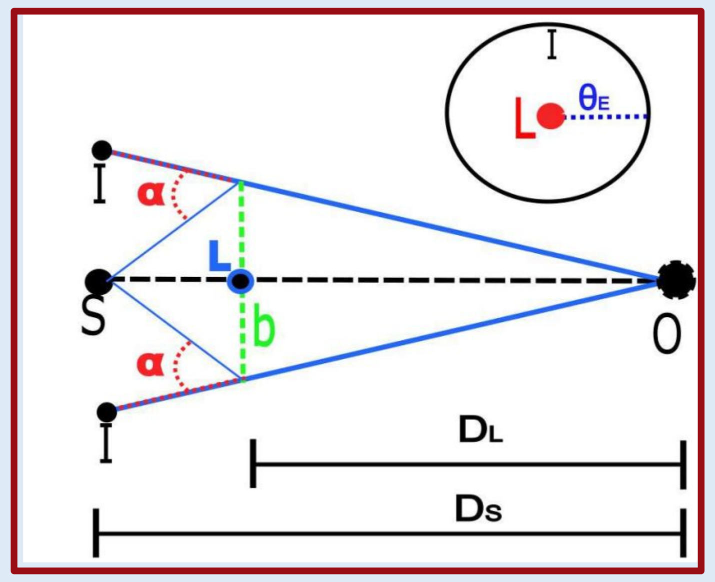


Fig.1 Annotated Gravitational lens geometry. O is the observer, S the source star, L the lens object, I the image positions, $D_L$ the distance to the Lens, $D_S$ the distance to the source

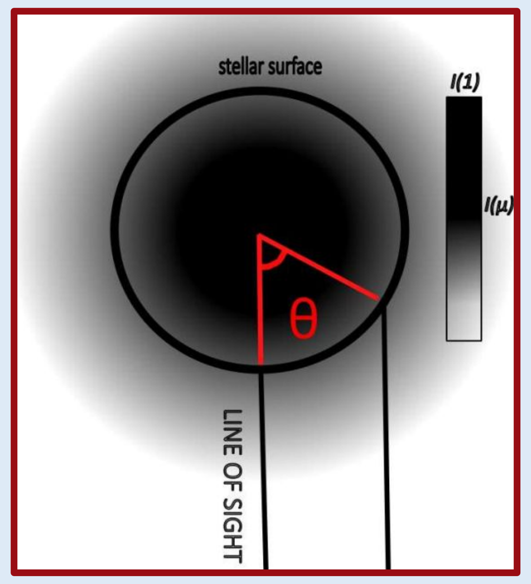


Fig.2 Annotated diagram explaining limb darkening. The center corresponds to the maximum I(1)=ξ(0). Different order parameterized profiles exist.

**Example: linear limb darkening Profile**

$$I(\mu) = \mathrm{I}(1)\left(1 - u(1-\mu)\right)$$

Where $\mu = \cos\theta$ , $\mathrm{I}(1) = \xi(0), \mathrm{I}(\mu) = \xi(\rho)$

## Motivation

**Importance of Limb Darkening:**

- Key parameter in **stellar atmospheric/evolution models - energy transport**, **opacity variations**, **temperature gradients**

**Limb Darkening in Microlensing vs Other Methods:**

- **Solar observations** - precise but **lack diversity**
- **Limb Darkening** depended: **spectral type**, **chemical composition**, **magnetic activity**
- **Transit photometry:**
  1. model priors → **biases**
  2. dimming effects → **complex disentanglement**
- **Microlensing: direct, unbiased, distant stars**, **non-parameterized limb darkening profiles**
- **Microlensing** →differential magnification→**no massive telescopes**

**Impact on Modern Astronomy:**

- **Bridge observational gaps** - solar studies, exoplanet/binary transits
- Powerful tool →**stellar atmospheric models, stellar evolution**

## Inversion Problem

Problem is an ill posed (singularity) inversion of a 1st order Fredholm integral

$$G_f(\eta;\,\xi) = \int_0^1 \mathcal{T}(\eta,\rho)\xi(\rho)d\rho$$

$$\mathcal{T}(\eta,\rho) = 2\,\rho^{\frac{1}{2}}\,j\left(\frac{\eta-1}{\rho}\right)$$

$G_f$ is the caustic profile function,
$\eta$ the caustic passage phase [0,2],
$\xi(\rho)$ the stellar intensity profile
$\mathcal{T}$ the kernel , $K$ the elliptical integral

$$j(z) = \begin{cases} 0 & \text{for } z \le -1 \\ \dfrac{2}{\sqrt{\pi}}K\left(\sqrt{\dfrac{1+z}{2}}\right) & \text{for } -1 < z < 1 \\ \dfrac{2}{\pi\sqrt{1+z}}K\left(\sqrt{\dfrac{2}{1+z}}\right) & \text{for } z \ge 1 \end{cases}$$

## Singularity

Fig.3,4 The singularities of kernel $\mathcal{T}$ shown as a $\mathcal{T}$ vs $\eta$ plot with varying $\rho$ and as a 2-D $\mathcal{T}(\eta,\rho)$ heatmap

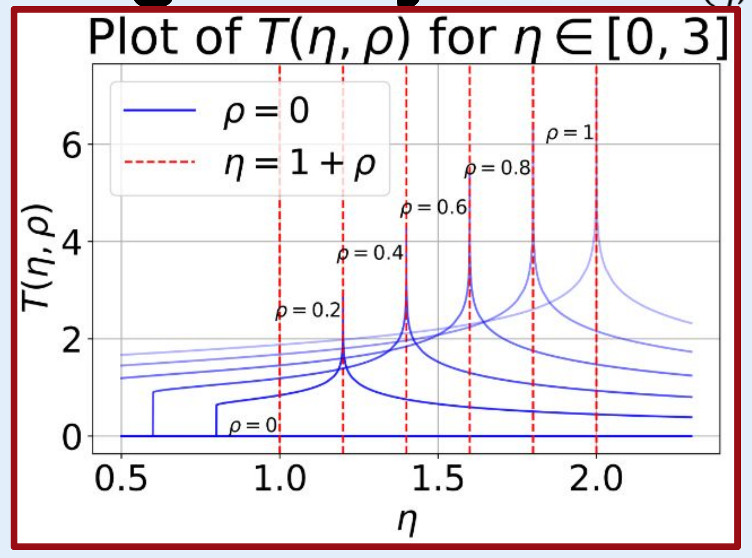


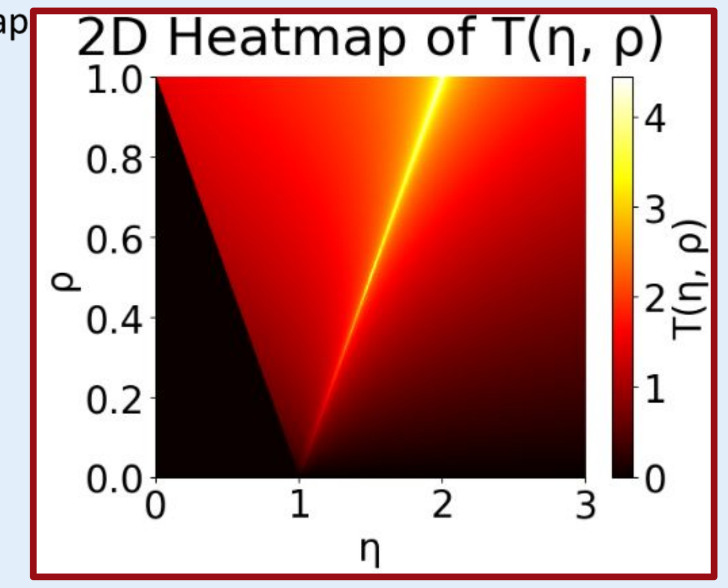


**PIM:**

$$G_f(\eta) = \sum_{j=1}^{N} \mathcal{T}(\eta_j,\rho_j)\xi_j\Delta \mathrm{r}_j$$

$$\xi(\rho) = \xi_j \text{ for } r \in [r_j, r_{j+1}],\ \Delta\mathrm{r}_j = r_{j+1} - r_j$$

**Solving PIM:**

$$G = T\,\xi$$

Where G is $G_f$ vector, T the kernel matrix, $\xi$ the vector of unknown $\xi_i$ values

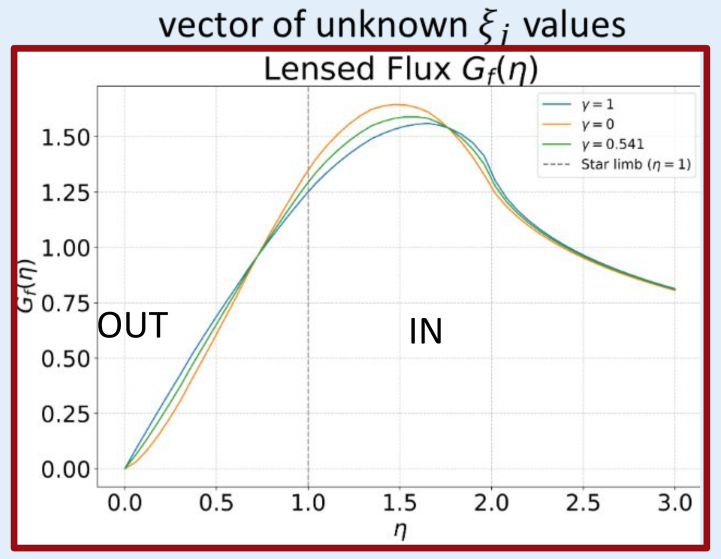


Fig.5 Plot of $G_f$ against the caustic crossing phase $\eta$, for different limb darkening profiles. Regions inside/outside the caustic are shown separated by the vertical line. These correspond to Fig.6

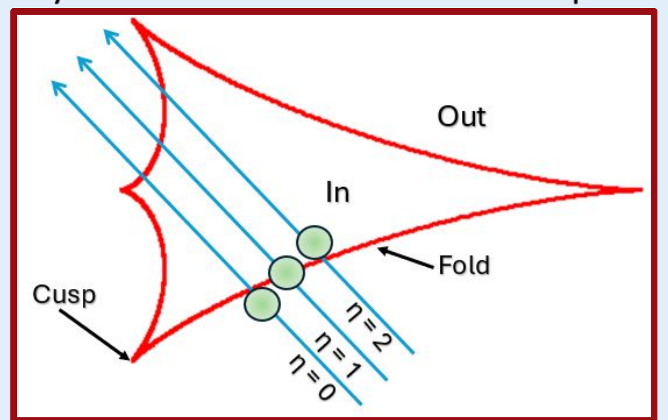


Fig.6 Annotated caustic in the abstract image plane. Annotated: 1.In/Out Regions, 2.Cusp/Fold caustic geometry, 3. Phase $\eta$ and corresponding positions

**B-spline Galerkin Approximation:**

$B_j$ are spline basis functions of $n^{th}$ degree

$$\xi(\rho) = \textstyle\sum_{j=1}^{N} c_j B_j(\rho)$$

$$G_f(\eta;\,\xi) = \int_0^1 \mathcal{T}(\eta,\rho)\sum_{j=1}^{N} c_j B_j(\rho)\,d\rho$$

$$\int_{\eta_o}^{\eta_f} B_i(\eta)G_f(\eta)\,d\eta$$

$$= \sum_{j=1}^{N} c_j \int_{\eta_o}^{\eta_f} B_i(\eta)\left(\int_0^1 \mathcal{T}(\eta,\rho)B_j(\rho)d\rho\right)d\eta$$

**FEM:**

$$\xi(\rho) = \textstyle\sum_{j=1}^{N} c_j\varphi_j(\rho)$$

$$\int_{\eta_o}^{\eta_f} \varphi_i(\eta)G_f(\eta)\,d\eta$$

$$= \sum_{j=1}^{N} c_j \int_{\eta_o}^{\eta_f} \varphi_i(\eta)\left(\int_0^1 \mathcal{T}(\eta,\rho)\varphi_j(\rho)d\rho\right)d\eta$$

$\varphi_j$ are triangular basis functions

$$\varphi_j(r) = \begin{cases} 1 - \left|\dfrac{r - r_j}{h}\right|, & r \in [r_{j-1}, r_{j+1}] \\ 0, & otherwise. \end{cases}$$

**Solving FEM/B-spline:**

$$b = A\,c$$

Where (here $B$ and $\varphi$ are interchangeable):
$b_i = \int_{\eta_o}^{\eta_f} B_i(\eta)G_f(\eta)\,d\eta$ (global load vector),
$A_{ij} = \int_{\eta_o}^{\eta_f} B_i(\eta)\left(\int_0^1 \mathcal{T}(\eta,\rho)B_j(\rho)d\rho\right)d\eta$ (global stiffness matrix)

## Recovered Profiles

Fig.7,8 The reconstructed profiles for each technique (left). The residuals, with a zoomed in region (right).

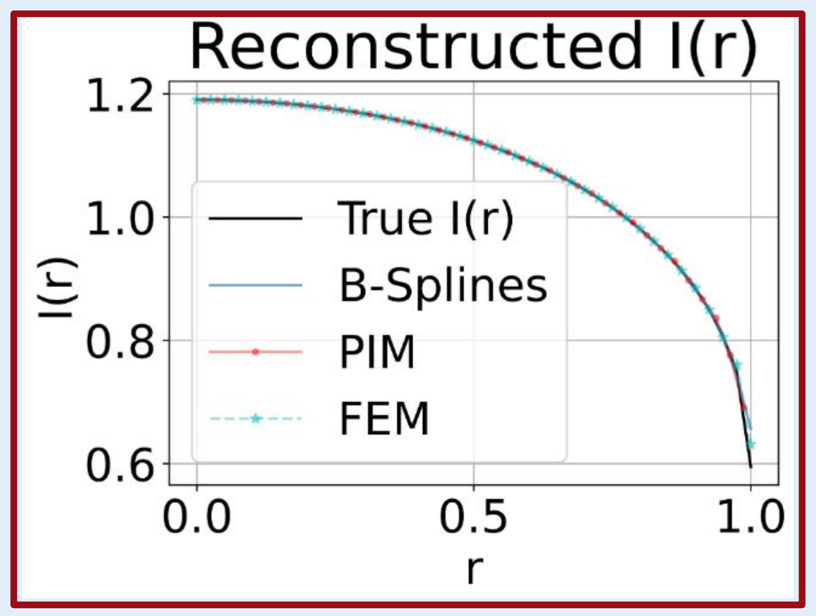


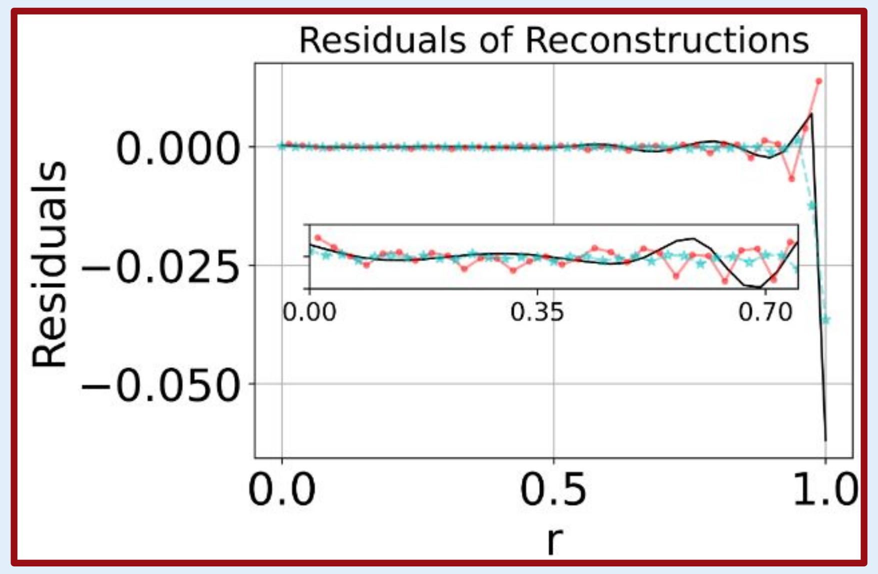


## Optimizing Algorithms

Ill poised problem sensitive to noise - containing singularity.
Standard inversion solutions unable to recover $\xi(\rho)$

**Optimize:**

- Custom7-stage **RKDP 5(4)** ODE solver →**adaptive step-size** control.
- Constrained solutions:
  1. Enforce $\xi_0 = \xi_1$ **flatness** in stellar center
  2. Enforce **negative monotonicity** $\xi_i - \xi_{i-1} \le 0 \quad \forall i$
  3. Enforce **negative concavity** $\xi_{i+1} - 2\xi_i + \xi_{i-1} \le 0 \quad \forall i$
- PIM sensitive to gaps in data/noise→**weighted Quadratic interpolation**
- Tune B-Spline→**grid search**→custom **sigmoid activation** function
- Test solvers (LU, LNNS, SLS, MOSEK)-**accuracy** and **efficiency**.
- **Perform Monte Carlo simulations to simulate "real data"(Gaussian noise)**

| Fit | (FEM) | (PIM) | B-splines |
|---|---|---|---|
| Gamma (0.45) | 0.379<br>0.445 | 0.443 | 0.386<br>0.439 |
| Beta (0.2) | 0.151<br>0.197 | 0.194 | 0.160<br>0.192 |

| Fit | (FEM) | (PIM) | B-splines |
|---|---|---|---|
| Gamma (0.83) | 0.716<br>0.827 | 0.83 | 0.662<br>0.75 |
| Beta (0.3) | 0.241<br>0.317 | 0.32 | 0.199<br>0.26 |

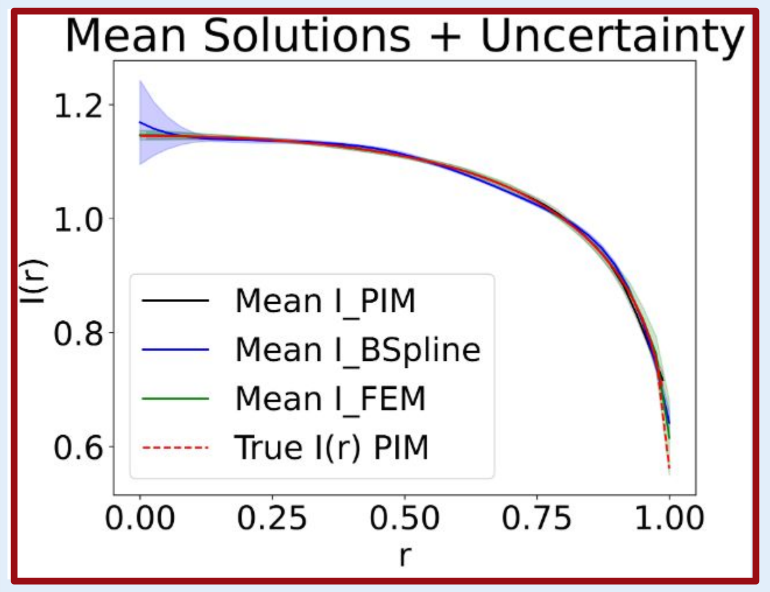


Fig.9 Mean reconstructed profile and standard deviation of Monte-Carlo simulation inverting noisy data.

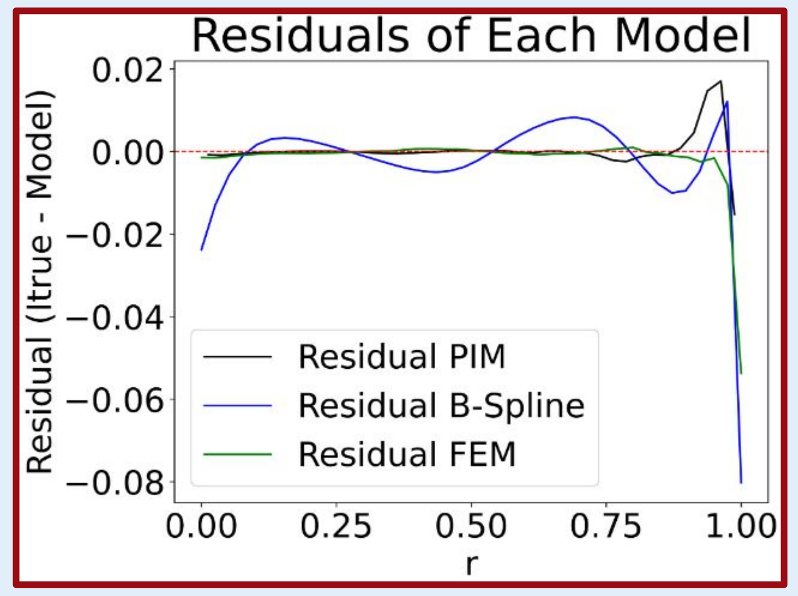


Fig.10 Residuals of fit. Unstable region close to r=1. (Also, near 0 for B-spline.) Tables showing recovered profiles params

## Discussion & Conclusion

**Results:**

- Recovery of nonparametric profiles using inversion methods.
- Power to distinguish between different order profiles.
- Noise heavily affects profile recovery

**Limitations:**

- Computational cost
- Use of real data requires recursion

**Future steps:**

1. Use of higher order FEM and more sophisticated techniques – computational cost
2. Construct recursion algorithm on real data, gradually recover non-parametric profile

**Acknowledgements:** I would like to thank my supervisor, Dr. Martin Dominik for his support in the early challenges in this project and his support. In addition, Dr. Laya Golchin for her advice in dealing with such an inversion problem.